Observation of electromigration in a Cu thin line by *in situ* coherent x-ray diffraction microscopy

Yukio Takahashi,[1,a)] Yoshinori Nishino,[2] Hayato Furukawa,[3] Hideto Kubo,[3] Kazuto Yamauchi,[3,4] Tetsuya Ishikawa,[2] and Eiichiro Matsubara[5]
[1]*Frontier Research Base for Global Young Researchers, Frontier Research Center, Graduate School of Engineering, Osaka University, 2-1 Yamada-oka, Suita, Osaka 565-0871, Japan*
[2]*RIKEN SPring-8 Center, Kouto, Sayo-cho, Sayo-gun, Hyogo 679-5148, Japan*
[3]*Department of Precision Science and Technology, Graduate School of Engineering, Osaka University, 2-1 Yamada-oka, Suita, Osaka 565-0871, Japan*
[4]*Research Center for Ultra-Precision Science and Technology, Graduate School of Engineering, Osaka University, 2-1 Yamada-oka, Suita, Osaka 565-0871, Japan*
[5]*Department of Materials Science and Engineering, Kyoto University, Yoshida, Sakyo, Kyoto 606-8501, Japan*

(Received 31 March 2009; accepted 12 May 2009; published online 25 June 2009)

Electromigration (EM) in a 1-μm-thick Cu thin line was investigated by *in situ* coherent x-ray diffraction microscopy (CXDM). Characteristic x-ray speckle patterns due to both EM-induced voids and thermal deformation in the thin line were observed in the coherent x-ray diffraction patterns. Both parts of the voids and the deformation were successfully visualized in the images reconstructed from the diffraction patterns. This result not only represents the first demonstration of the visualization of structural changes in metallic materials by *in situ* CXDM but is also an important step toward studying the structural dynamics of nanomaterials using x-ray free-electron lasers in the near future. © *2009 American Institute of Physics*. [DOI: 10.1063/1.3151855]

I. INTRODUCTION

Atomic diffusion caused by momentum transfer from conducting electrons is a phenomenon known as electromigration (EM).[1] Under a high current density of $\sim 10^6$ A/cm^2, voids and hillocks form around the interconnecting wires due to EM and often result in the failure of Cu wiring layers in large-scale integration (LSI) circuits.[2,3] To enhance the reliability of LSI circuits and design new LSI structures, understanding the mechanism of deterioration in Cu wiring layers is important. The evaluation of structural changes in wiring layers induced by EM has been carried out by electron microscopy, x-ray microscopy,[4,5] and x-ray microdiffraction.[6] Transmission electron microscopy (TEM) is a well-established microscopy technique with atomic resolution. Recently, EM-induced surface atomic steps in Cu lines have been observed by *in situ* TEM.[7] TEM is a powerful tool for evaluating local structures in metallic foils thinner than a few hundred nanometers. Hard x-ray microscopy equipped with a Fresnel zone plate is a promising method of x-ray microscopy and was recently developed at synchrotron x-ray radiation facilities, which can currently achieve about 30 nm resolution.[8] Until now, both Cu thin lines and EM-induced voids in a LSI structure has been three-dimensionally observed by hard x-ray tomographic microscopy.[9,10] Mass transport of the early stages of EM in a Cu line has been investigated by dynamical x-ray microscopy.[5] Polychromatic microdiffraction equipped with Kirkpatrick–Baez mirrors is also a powerful tool for characterizing mesoscopic length scale structures of polycrystalline materials.[6] Until now, grain orientation,[11] plastic deformation,[12] dislocation arrangement,[13] and grain deformation and rotation[14] induced by EM on interconnects have been evaluated by the microdiffraction technique. However, it is difficult for these x-ray techniques to observe samples with nanometer-scale resolution due to the fabrication limit of x-ray optical devices. *In situ* coherent x-ray diffraction microscopy (CXDM), which is first demonstrated in the present study, is a promising tool for observing EM-induced structural changes in micrometer-thick lines with nanometer-scale resolution.

CXDM[15–18] is a fairly new lensless x-ray imaging technique using coherent x-ray scattering. The sample is illuminated by x rays with a well-defined wave front, and its diffraction pattern is measured. Images are derived by applying phase retrieval algorithms[19–21] to the diffraction pattern. In principle, the spatial resolution of CXDM is half of the wavelength of the incident x rays. The first implementation of CXDM was reported by Miao *et al.* in 1999.[15] Subsequently, various CXDM studies have been performed in experiments using synchrotron radiation,[22–28] table-top high-harmonic soft x rays,[29] and a vacuum ultraviolet free-electron laser.[30–32] Many researchers planned to carry out CXDM using x-ray free-electron lasers (XFELs), which are a next-generation x-ray source under construction at several facilities around the world. The XFEL is predicted to provide extremely intense femtosecondpulse x rays with almost full spatial coherence. CXDM is therefore expected to establish a new frontier in structural dynamics studies of nanomaterials. For example, *in situ* CXDM can be used to study the dynamics of precipitates and/or pore growth or shrinkage during material processing.[33] In the present article, we report the first visualization of EM in a Cu thin line by *in situ* CXDM,

[a)]Author to whom correspondence should be addressed. Electronic mail: takahashi@wakate.frc.eng.osaka-u.ac.jp.

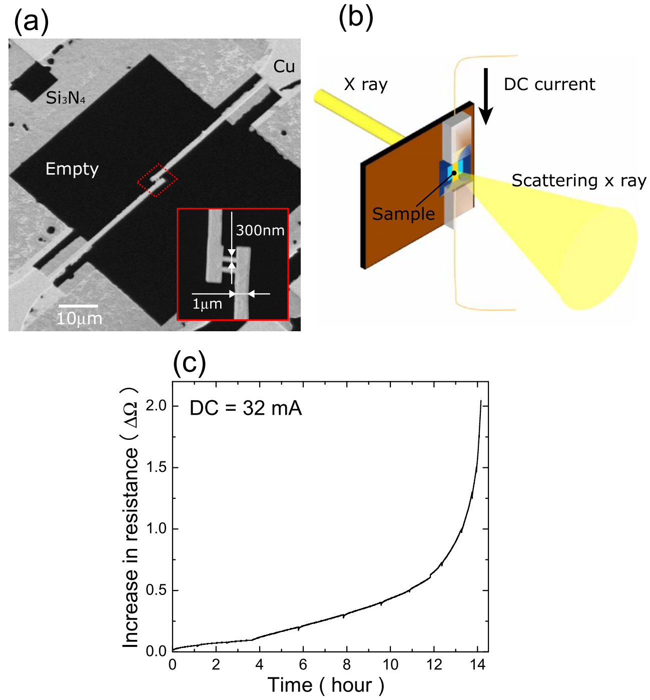

FIG. 1. (Color online) (a) SEM image of the Cu thin line fabricated on a SiN membrane chip. (b) Schematic of the system used for applying dc to the thin line sample during CXDM measurements. (c) Time dependence of the increase in resistance of the Cu thin line when a dc of 32 mA was applied.

which has been developed at SPring-8, as an important step toward the use of XFELs.

II. EXPERIMENT

Figure 1(a) shows a scanning electron microscope (SEM) image of the Cu thin line sample. A 1-μm-thick Cu film was deposited on a 270-nm-thick SiN membrane by electron-beam evaporation using a mask.[34] 1-μm-wide thin lines and 300-nm-wide adjacent connections, which simulate via structures in LSI circuits, were fabricated in the Cu film using a focused ion beam. The Cu/SiN in a $60\times60\ \mu\text{m}^2$ area around the connections was completely removed to avoid scattering x rays from the membrane. Figure 1(b) shows a schematic of the system used for applying dc to the thin line sample during the CXDM measurements. The SiN membrane chip supporting the Cu thin line was held between a Bakelite base and acrylic resin clips. The sample holder was mounted on a stage in the vacuum chamber. A dc of 32 mA was applied to the Cu thin line via Cu wires from outside the chamber. Estimated current density was $3.2\times10^6\ \text{A/cm}^2$ for the 1-μm-wide thin lines and $5.3\times10^6\ \text{A/cm}^2$ for the 300-nm-wide adjacent connections. Figure 1(c) shows the time dependence of the increase in resistance. When the resistance increased by 0, 0.05, 0.1, 0.3, 0.7, 1.0, 1.5, and 2.0 Ω, the application of dc was temporarily stopped to measure coherent x-ray diffraction patterns. These measurements were carried out at BL29XUL (Ref. 34) in SPring-8, Japan 5 keV x rays irradiated the thin line including the adjacent connections through a 20 μm pinhole slit. The lateral coherence length of the incident x rays at the sample position is considered to be similar to the beam size along the vertical direction and ~5 μm along the horizontal direction. To illuminate the thin line by x rays with better coherence, the sample was mounted on a stage so that the longitudinal direction of the thin line was in the vertical direction, as shown in Fig. 1(b). The experimental setup for the CXDM measurements is similar to that described in our previous report.[35] Forward x-ray diffraction intensities were collected using an in-vacuum frontside-illuminated charge-coupled device (CCD) detector with a pixel size of $20\times20\ \mu\text{m}^2$ that was placed 2.924 m downstream of the sample. Guard slits were used to suppress parasitic x rays scattered from the pinhole. A direct beamstop was positioned in front of the CCD detector. It took 6.3 h to collect the data of each diffraction pattern. The exposure time of x rays was 2.7 h, where 2.2 h were for the sample measurement and 0.5 h was for the background measurement. The total readout time from the CCD was 3.6 h.

III. RESULTS AND DISCUSSION

Figures 2(a)–2(d) show the coherent x-ray diffraction patterns of the Cu thin lines when the increases in resistance were Δ0.3, Δ0.7, Δ1.5, and Δ2.0 Ω. To the right of each diffraction pattern, a closeup of the pattern surrounded by a white square is displayed in a different color. Since the diffraction patterns measured at Δ0, Δ0.05, Δ0.1, and Δ0.3 Ω were almost identical and those at Δ1.0 and Δ1.5 Ω were also the same, these diffraction patterns are represented by those at Δ0.3 and Δ1.5 Ω, respectively, in Fig. 2. In the diffraction pattern at Δ0.3 Ω, the speckle patterns spreading to the upper right and lower left result from the 300-nm-wide adjacent connections in the sample. Similar speckle patterns can also be seen in the other diffraction patterns. The direction in which the speckle patterns spread rotates clockwise as the resistance increases, which is schematically drawn in Fig. 2(e). This implies that the adjacent connections leaned right as the resistance increased. In the diffraction patterns at Δ0.7 Ω and higher, characteristic speckle patterns that were not observed at Δ0.3 Ω can be seen in the upper left and lower right directions. A part of the characteristic speckles is colored and the directions are shown by dotted lines. The process of change in both the speckles and the directions is schematically drawn in Fig. 2(e). The size of the speckles decreases as the resistance increases. The direction in which the speckle patterns spread and the speckles themselves rotate counterclockwise as the resistance increases. This implies that a characteristic structure was produced in the thin line between Δ0.3 and Δ0.7 Ω, and its size increased and shape changed as the resistance increased. The coherent x-ray diffraction intensity corresponds to the magnitude of the Fourier transformation of the projection image of the sample. Both the size and shape of the structure can be estimated from the characteristic speckle. Table I summarizes the estimated structures. The structure is an EM-induced void in the thin line. Many line-shaped speckles can be seen in the diffraction pattern at Δ0.3 Ω, as indicated by the black arrows in Fig. 2(a). As the resistance increases, the line-

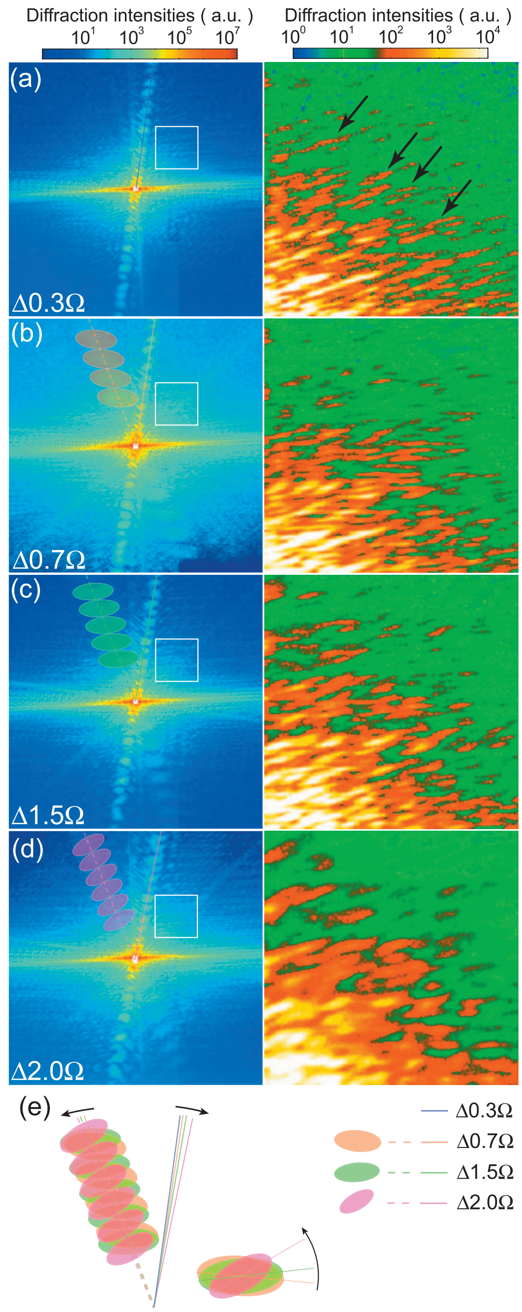

FIG. 2. (Color) Coherent x-ray diffraction patterns of the Cu thin line in 1201×1201 pixels when the increases in resistance are (a) Δ0.3, (b) Δ0.7, (c) Δ1.5, and (d) Δ2.0 Ω. The pixel size is 1.73×10^{-4} nm^{-1}. To the right of each diffraction pattern, a closeup of the pattern in 200×200 pixels surrounded by the white square is displayed in a different color. The central $\sim25\times25$ pixels, which are displayed in white, are not measured due to the beamstop. The directions of speckle patterns spreading to the upper right are traced by solid lines. In the patterns of (b)–(d), speckle patterns spreading to the upper left are colored, and the directions are traced by dotted lines. (e) The relationship between the colored speckles and the lines traced in (a)–(d) is schematically drawn.

shaped speckles disappear, and the large speckles are produced, which implies that the width of a part of the thin line decreased as the resistance increased.

To evaluate the process of the EM-induced structural changes in the thin line, images were reconstructed from the diffraction patterns. Even if the sample is one-dimensionally long such as the thin line, when it has a specific structure that

TABLE I. Relationship between the characteristics speckles observed at Δ0.7, Δ1.5, and Δ2.0 Ω and the objects estimated from the speckles.

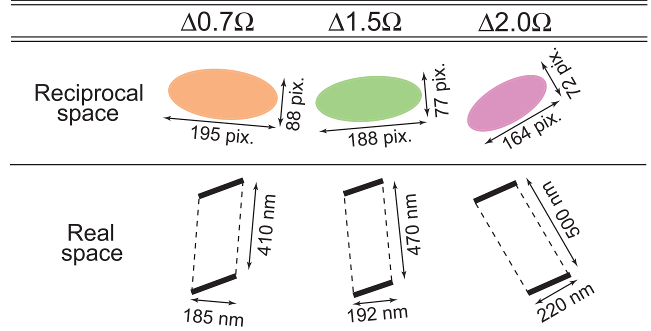

is the ladderlike shape in the present sample and the two-dimensional oversampling ratio, which was ~25 in the present measurement, is more than 2, it is possible to reconstruct sample images by using an exact support which is the nonzero region in the real space.[36] The reconstruction was carried out by the following procedure: (i) a random-complex-number array in real space was generated with a size of 1201×1201 pixels. A fast Fourier transform (FFT) was applied to the real-space array. The magnitudes of the output complex values in the experimentally measured region were replaced with the diffraction data, while the maximum value of the diffraction data was set in every pixel of the central region, which was unmeasured region because of the presence of a direct beamstop.[37] Next, an inverse FFT (IFFT) was applied to the complex values. The resultant real-space array is the initial image. The support was initially derived from the SEM image. (ii) A real-space constraint of Fienup's hybrid input-output algorithm[20] is applied to the real-space array. An FFT is then applied to the real-space array. (iii) The magnitudes of the output complex values in the experimentally measured region were replaced with the diffraction data. An IFFT was applied to the complex values. Steps (ii) and (iii) are repeated 10 000 times. The magnitudes of ten independent complex images, i.e., $|\rho_1|,|\rho_2|,\ldots,|\rho_{10}|$, were reconstructed. The reconstruction error ($R_{i,j}$) of two independent images ($|\rho_i|$ and $|\rho_j|$), $R_{i,j}=\Sigma(|\rho_i|-|\rho_j|)/\Sigma(|\rho_i|+|\rho_j|)$, was used to evaluate the reliability of the reconstruction process. The support was manually modified so that the error decreased. The five most similar $|\rho|$ images were averaged to produce the final image. It was considered that $|\rho|$ is almost proportional to the projection of the electron-density distribution of the sample. $R_{i,j}$ values of each final image were ~10%. The reconstruction error is slightly large compared to that in previous experiments on a completely isolated sample. It is likely that the imperfect reconstruction is due to the reduction in the contrast of the interference intensities caused by the intensity integration over the CCD pixels,[38] the illumination of the sample by partially coherent x rays,[39] and the curved beam illumination from the pinhole. Although the reconstruction was imperfect, it was confirmed by a simulation that voids around the ladderlike shape can be visualized.

Figures 3(a) and 3(b) show SEM images of the thin line observed before and after measuring all the diffraction patterns, respectively. EM-induced voids are formed at dark ar-

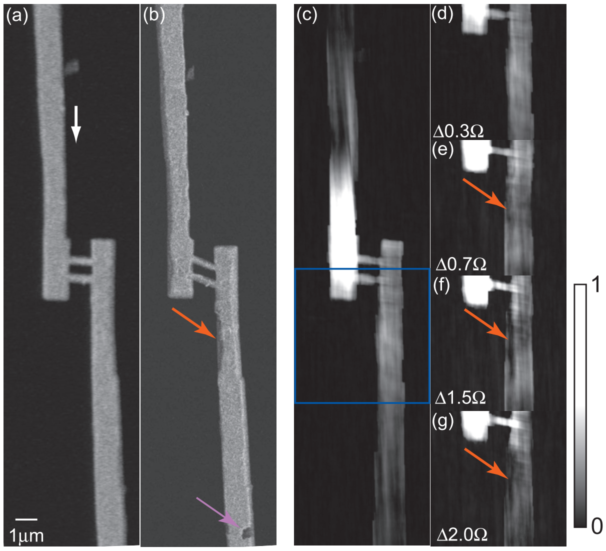

FIG. 3. (Color) [(a) and (b)] SEM images of the Cu thin line observed (a) before and (b) after measuring all the diffraction patterns. A dc was applied to the thin line from the upper side along the white arrow. (c) Image in 200×800 pixels reconstructed from diffraction pattern of Fig. 2(a). The pixel size is 30.2 nm. The image is displayed in grayscale. [(d)–(g)] Images in 200×200 pixels reconstructed from diffraction patterns of Figs. 2(a)–2(d), respectively, in the area surrounded by the blue square in (c). Pixels with intensity greater than 50% of the maximum intensity in each reconstructed image are displayed in white.

eas indicated by red and pink arrows in Fig. 3(b). The adjacent connection of the thin line is distorted in comparison with that in Fig. 3(a). Figure 3(c) shows the image reconstructed from the diffraction pattern at Δ0.3 Ω. The image is displayed in grayscale. The white color corresponds to higher-density regions, while the black color corresponds to lower-density regions. Part of the reconstructed image is unrealistically bright. This is thought to be due to both the intensity integration over the CCD pixels[38] and the insufficient x-ray coherence.[39] This tendency was also seen in the images reconstructed from the diffraction patterns at other resistances. The size and shape of the void indicated by the pink arrow in Fig. 3(b) are consistent with those of the estimated object shown at Δ2.0 Ω in Table I. The characteristic speckles seen in Figs. 2(a)–2(d) therefore result from the void, although the real image was not reconstructed. Figures 3(d)–3(g) show the images reconstructed from the diffraction patterns in Figs. 2(a)–2(d), respectively. The area surrounded by the blue square in Fig. 3(c) is displayed. The images were normalized by the summation of intensities in each image. The adjacent connection gradually leans to the lower right as the resistance increases, which is almost consistent with the estimation from the diffraction patterns. The deformation is thought to be due to the thermal stress induced by current heating. A black region can be seen at the position indicated by the red arrow in the reconstructed image at Δ0.7 Ω, which is similar to the area of the EM-induced void seen in the SEM image. At Δ1.5 Ω, the black region extends in the longitudinal direction. At Δ2.0 Ω, the black region is slightly larger. It is clear that the black region corresponds to the EM-induced void. The growth process of the line-shaped void is successfully visualized in the reconstructed images. In addition, it was confirmed by a simulation that the change in the line-shaped speckles seen in Fig. 2 is due to the reduction in the Cu linewidth at the area indicated by the red arrow.

The average brilliance of x rays radiated from in-vacuum undulator installed at BL29XUL in SPring-8 is $\sim10^{20}$ (photons/mm^2 mrad^2 s in 0.1% bandwidth),[40] while that of the Japanese XFEL is estimated to be $\sim10^{21}$ (photons/mm^2 mrad^2 s in 0.1% bandwidth).[41] Therefore, if the dynamic range of CCD detectors is improved and the readout time becomes short, the diffraction data can be collected quickly ten times. Moreover, coherent high dense x rays can be produced by focusing XFEL because it has almost full spatial coherence. When x-ray beams are focused, the x-ray illumination area becomes small. For the present method, the maximum value of the size of samples is limited by the focusing spot size. Therefore, according to the size of samples, it is effective to use ptychography[27] or keyhole imaging.[28] As the result, measurement time can be shortened further. On the other hand, radiation damage of the sample will be serious. When the sample is irradiated by high-peak brilliance x rays such as XFEL pulse x rays, it is not understood how the sample is changed. At least, metallic samples should be more resistant to radiation than biological samples.

In the present study, the small angle x-ray scattering data were collected, which offered electron density distribution of the Cu thin line, while the coherent diffraction intensity data near the Bragg peaks offer strain distribution in addition to electron density distribution.[16] For the latter method, the sample is limited to the single crystal or the single grain in a polycrystal. For polycrystalline samples such as the present thin line, CXDM using Bragg peaks is useful to evaluate local structures in samples, such as strain distribution in a single grain near an interconnect.

IV. CONCLUSION

In situ CXDM under the application of a dc was developed at SPring-8 as a step toward the use of XFELs and was applied to evaluate EM in a 1-μm-thick Cu thin line. Both EM-induced voids and thermal deformation in the thin line were made to appear characteristic x-ray speckle patterns in the coherent x-ray diffraction patterns, which were successfully visualized in the images reconstructed from the diffraction patterns. The present result not only represents the first demonstration of the visualization of structural changes in metallic materials by *in situ* CXDM but is also an important step toward studying the structural dynamics of nanomaterials using XFELs in the near future. To trace faster EM process and to examine the three-dimensional structure of EM-induced voids with better resolution, it is necessary to use more brilliant and almost fully coherent x rays such as those from XFEL. We believe that *in situ* CXDM will be established as a technique for evaluating EM in LSI circuits in the near future.

ACKNOWLEDGMENTS

This research has been carried out at the Frontier Research Base for Global Young Researchers, Osaka University, on the Program of Promotion of Environmental Improvement to Enhance Young Researcher's Independence, the Special Coordination Funds for Promoting Science and Technology, from the Ministry of Education, Culture, Sports, Science and Technology (MEXT). This work was also partly supported by funds from a Grant-in-Aid for Scientific Research (B) (Grant Nos. 18360304 and 19310084), Specially Promoted Research (Grant No. 18002009), Young Scientists (Grant No. 21686060), the Global COE Program "Center of Excellence for Atomically Controlled Fabrication Technology," and the "Promotion of X-ray Free Electron Laser Research" from MEXT, Konica Minolta Imaging Science Fundation, and Shimadzu Science Fundation.

[1]H. B. Huntington and A. R. Grone, J. Phys. Chem. Solids **20**, 76 (1991).
[2]L. Arnaud, T. Berger, and G. Reimbold, J. Appl. Phys. **93**, 192 (2003).
[3]E. Liniger, C.-K. Hu, L. M. Gignac, and A. Simon, J. Appl. Phys. **93**, 9576 (2003).
[4]J. T. Lau, J. A. Prybyla, and S. K. Theissb, Appl. Phys. Lett. **76**, 164 (2000).
[5]G. Schneider, G. Denbeaux, E. H. Anderson, B. Bates, A. Pearson, M. A. Meyer, E. Zschech, D. Hambach, and E. A. Stach, Appl. Phys. Lett. **81**, 2535 (2002).
[6]N. Tamura, R. S. Celestre, A. A. MacDowell, H. A. Padmore, R. Spolenak, B. C. Valek, N. Meier Chang, A. Manceau, and J. R. Patel, Rev. Sci. Instrum. **73**, 1369 (2002).
[7]K.-C. Chen, C.-N. Liao, W.-W. Wu, and L.-J. Chen, Appl. Phys. Lett. **90**, 203101 (2007).
[8]G.-C. Yin, Y.-F. Song, M.-T. Tang, F.-R. Chen, K. S. Liang, F. W. Duewer, M. Feser, and W. Yun, Appl. Phys. Lett. **89**, 221122 (2006).
[9]Z. H. Levine, A. R. Kalukin, S. P. Frigo, I. McNulty, and M. Kuhn, Appl. Phys. Lett. **74**, 150 (1999).
[10]Z. H. Levine, A. R. Kalukin, M. Kuhn, S. P. Frigo, I. McNulty, C. C. Retsch, Y. Wang, U. Arp, T. B. Lucatorto, B. D. Ravel, and C. Tarrio, J. Appl. Phys. **87**, 4483 (2000).
[11]N. Tamura, A. A. MacDowell, R. S. Celestre, H. A. Padmore, B. C. Valek, J. C. Bravman, R. Spolenak, W. L. Brown, T. Marieb, H. Fujimoto, B. W. Batterman, and J. R. Patel, Appl. Phys. Lett. **80**, 3724 (2002).
[12]R. I. Barabash, G. E. Ice, N. Tamura, B. C. Valek, J. C. Bravman, R. Spolenak, and J. R. Patel, J. Appl. Phys. **93**, 5701 (2003).
[13]A. S. Budiman, W. D. Nix, N. Tamura, B. C. Valek, K. Gadre, J. Maiz, R. Spolenak, and J. R. Patel, Appl. Phys. Lett. **88**, 233515 (2006).
[14]Kai Chen, N. Tamura, B. C. Valek, and K. N. Tu, J. Appl. Phys. **104**, 013513 (2008).
[15]J. Miao, P. Charalambous, J. Kirz, and D. Sayre, Nature (London) **400**, 342 (1999).
[16]M. A. Pfeifer, G. J. Williams, I. A. Vartanyants, R. Harder, and I. K. Robinson, Nature (London) **442**, 63 (2006).
[17]P. Thibault, M. Dierolf, A. Menzel, O. Bunk, C. David, and F. Pfeiffer, Science **321**, 379 (2008).
[18]B. Abbey, K. A. Nugent, G. J. Williams, J. N. Clark, A. G. Peele, M. A. Pfeifer, M. de Jonge, and I. McNulty, Nat. Phys. **4**, 394 (2008).
[19]R. W. Gerchberg and W. O. Saxton, Optik (Stuttgart) **35**, 237 (1972).
[20]J. R. Fienup, Appl. Opt. **21**, 2758 (1982).
[21]V. Elser, J. Opt. Soc. Am. A **20**, 40 (2003).
[22]J. Miao, K. O. Hodgson, T. Ishikawa, C. A. Larabell, M. A. LeGros, and Y. Nishino, Proc. Natl. Acad. Sci. U.S.A. **100**, 110 (2003).
[23]D. Shapiro, P. Thibault, T. Beetz, V. Elser, M. Howells, C. Jacobsen, J. Kirz, E. Lima, H. Miao, A. M. Neiman, and D. Sayre, Proc. Natl. Acad. Sci. U.S.A. **102**, 15343 (2005).
[24]J. Miao, C.-C. Chen, C. Song, Y. Nishino, Y. Kohmura, T. Ishikawa, D. Ramunno-Johnson, T.-K. Lee, and S. H. Risbud, Phys. Rev. Lett. **97**, 215503 (2006).
[25]G. J. Williams, H. M. Quiney, B. B. Dhal, C. Q. Tran, K. A. Nugent, A. G. Peele, D. Paterson, and M. D. de Jonge, Phys. Rev. Lett. **97**, 025506 (2006).
[26]Y. Takahashi, Y. Nishino, T. Ishikawa, and E. Matsubara, Appl. Phys. Lett. **90**, 184105 (2007).
[27]J. M. Rodenburg, A. C. Hurst, A. G. Cullis, B. R. Dobson, F. Pfeiffer, O. Bunk, C. David, K. Jefimovs, and I. Johnson, Phys. Rev. Lett. **98**, 034801 (2007).
[28]B. Abbey, K. A. Nugent, G. J. Williams, J. N. Clark, A. G. Peele, M. A. Pfeifer, M. de Jonge, and I. McNulty, Nat. Phys. **4**, 394 (2008).
[29]R. L. Sandberg, A. Paul, D. A. Raymondson, S. Hädrich, D. M. Gaudiosi, J. Holtsnider, R. I. Tobey, O. Cohen, M. M. Murnane, H. C. Kapteyn, C. Song, J. Miao, Y. Liu, and F. Salmassi, Phys. Rev. Lett. **99**, 098103 (2007).
[30]H. N. Chapman, A. Barty, M. J. Bogan, S. Boutet, M. Frank, S. P. Hau-Riege, S. Marchesini, B. W. Woods, S. Bajt, W. H. Benner, R. A. London, E. Plönjes, M. Kuhlmann, R. Treusch, S. Düsterer, T. Tschentscher, J. R. Schneider, E. Spiller, T. Möller, C. Bostedt, M. Hoener, D. A. Shapiro, K. O. Hodgson, D. V. D. Spoel, F. Burmeister, M. Bergh, C. Chaleman, G. Huldt, M. M. Seibert, F. R. N. C. Maia, R. W. Lee, A. Szöke, N. Timneanu, and J. Hajdu, Nat. Phys. **2**, 839 (2006).
[31]M. J. Bogan, W. H. Benner, S. Boutet, U. Rohner, M. Frank, A. Barty, M. M. Seibert, F. Maia, S. Marchesini, S. Bajt, B. Woods, V. Riot, S. P. Hau-Riege, M. Svenda, E. Marklund, E. Spiller, J. Hajdu, and H. N. Chapman, Nano Lett. **8**, 310 (2008).
[32]A. Barty, S. Boutet, M. J. Bogan, S. Hau-Riege, S. Marchesini, K. Sokolowski-Tinten, N. Stojanovic, R. Tobey, H. Ehrke, A. Cavalleri, S. Düsterer, M. Frank, S. Bajt, B. W. Woods, M. M. Seibert, J. Hajdu, R. Treusch, and H. N. Chapman, Nature Photon. **2**, 415 (2008).
[33]Technical design report of the European XFEL (http://xfel.desy.de/tdr/tdr).
[34]K. Tamasaku, Y. Tanaka, M. Yabashi, H. Yamazaki, N. Kawamura, M. Suzuki, and T. Ishikawa, Nucl. Instrum. Methods Phys. Res. A **467–468**, 686 (2001).
[35]Y. Takahashi, H. Furukawa, H. Kubo, K. Yamauchi, Y. Nishino, T. Ishikawa, and E. Matsubara, Surf. Interface Anal. **40**, 1046 (2008).
[36]L.-M. Stadler, R. Harder, I. K. Robinson, C. Rentenberger, H. P. Karnthaler, B. Sepiol, and G. Vogl, Phys. Rev. B **76**, 014204 (2007).
[37]Y. Nishino, J. Miao, and T. Ishikawa, Phys. Rev. B **68**, 220101(R) (2003).
[38]C. Song, D. Ramunno-Johnson, Y. Nishino, Y. Kohmura, T. Ishikawa, C.-C. Chen, T.-K. Lee, and J. Miao, Phys. Rev. B **75**, 012102 (2007).
[39]I. A. Vartanyants and I. K. Robinson, J. Phys.: Condens. Matter **13**, 10593 (2001).
[40]See light sources overview in SPring-8 website http://www.spring8.or.jp.
[41]See light sources overview in SPring-8 Joint Project for XFEL website http://www.riken.jp/XFEL/eng/index.html.